Imaging the deep roots of the San Andreas Fault Zone at Parkfield, CA, with magnetotelluric measurements

M. Becken, O. Ritter, U. Weckmann, W. Wilhelms, J. Hübert, T. Branch, P. Bedrosian, S. Park and M. Weber

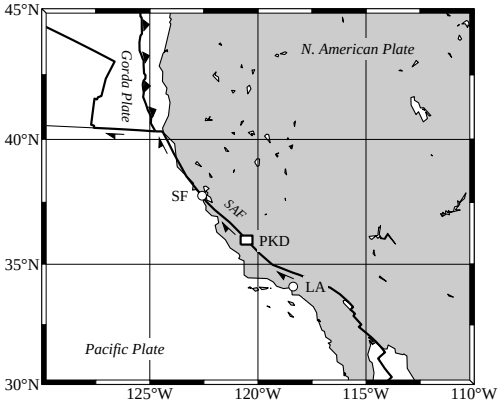

Figure 1: Map of western North America. The San Andreas Fault zone separates the Pacific and the North American Plates. Arrows indicate the right-lateral motion along the transform fault with a velocity of app. $4.9\,cm/a$. The box in the central part of the map indicates the working area near Parkfield, CA. SF San Francisco; LA Los Angelos; PKD Parkfield.

Introduction

With the magnetotelluric (MT) project DeepRoot, we aim to image the electrical conductivity distribution of the deep structures (brittle-ductile transition zone and the ductile roots) of the San Andreas Fault (SAF) zone at Parkfield, CA (Figure 1). The experiment addresses the dynamics of interplate transform faulting and contributes to the site characterisation of the San Andreas Fault Observatory At Depth (SAFOD) - a major Earth Science initiative to study the in-situ physical and chemical conditions of the San Andreas interplate transform fault (Hickman et al., 2004). The project DeepRoot is part of the ICDP.

Previous MT studies of Unsworth and Bedrosian (2004) played an important role to pin-point the location of the SAFOD site. The electrical conductivity models from these studies suggested the presence of fluids, causative for the so-called fault zone conductor (FZC) on the northeastern side of the fault (North-American plate) and thereby provided complementary information to the seismic velocity structure and other geophysical site characterisation studies. It was a remarkable observation that the FZC occupies a volume with abundant seismicity. As fluids seem to be intimately linked to the brittle deformation processes within active fault zones, the FZC was interpreted in terms of over-pressured fluids, which in turn prevent the fault from rupturing. From borehole fluid pressure measurements in the SAFOD well, however, it was recognised, that fluids are over-pressured on the Pacific plate and under-pressured on the North American plate. This was an unexpected result taking into account the MT model.

The previous MT models were limited to a few kilometres in depth due to short profile lengths. In spring 2005, we acquired a huge volume of new magnetotelluric (MT) data on a $50 \times 50\text{km}^2$array and and a 50km long profile in the vicinity of the SAFOD site. Overall, we recorded at 45 combined long-period / broad-band stations additional 41 broad-band stations along a profile coincident with a 50 km long seismic reflection/refraction profile (Hole et al., 2004; Ryberg et al., 2004). The profile data were used to derive a two-dimensional (2D) electrical conductivity model down to a depth of more than 25 km. The array data will give us the unprecedented opportunity to develop a three-dimensional (3D) electrical conductivity model in the surrounding of the SAFOD (see Figure 2). In this contribution, we discuss the profile data only, because processing and analysis of the array data is not yet completed.

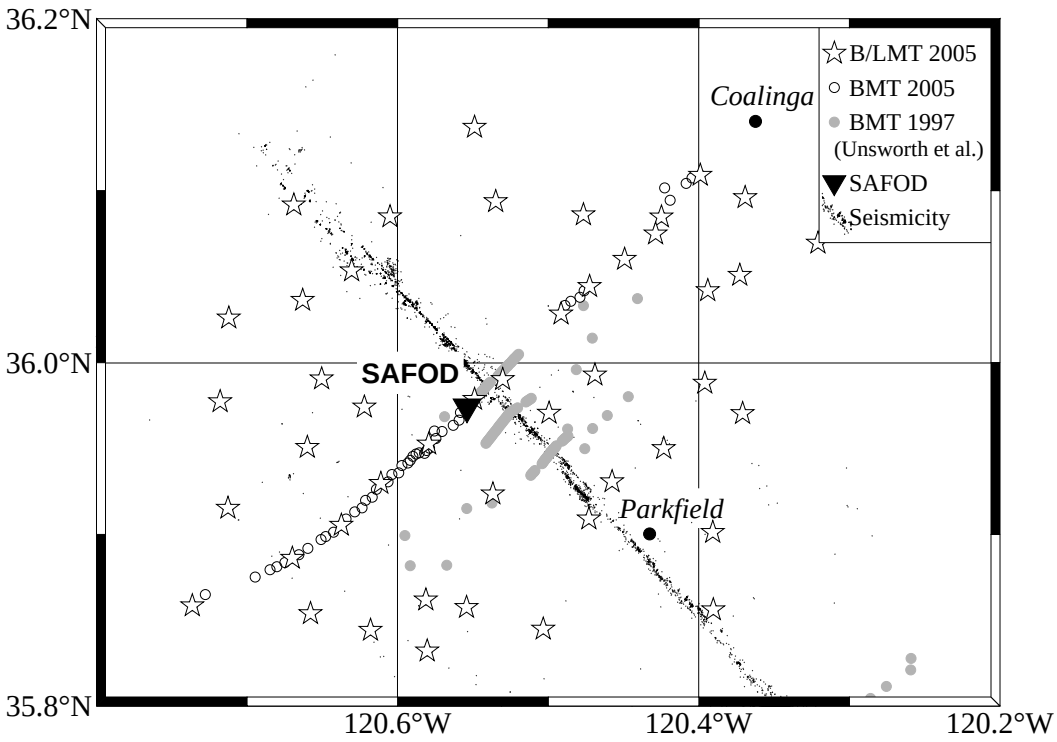

Figure 2: MT sites in the Parkfield area. New broad-band sites (BMT) are shown as hollow circles; new combined broad-band/long-period sites (B/LMT) are indicated by hollow stars. Existing BMT data from Unsworth et al. (1997) are shown as gray dots. The seismicity along the San Andreas Fault zone is depicted with black dots.

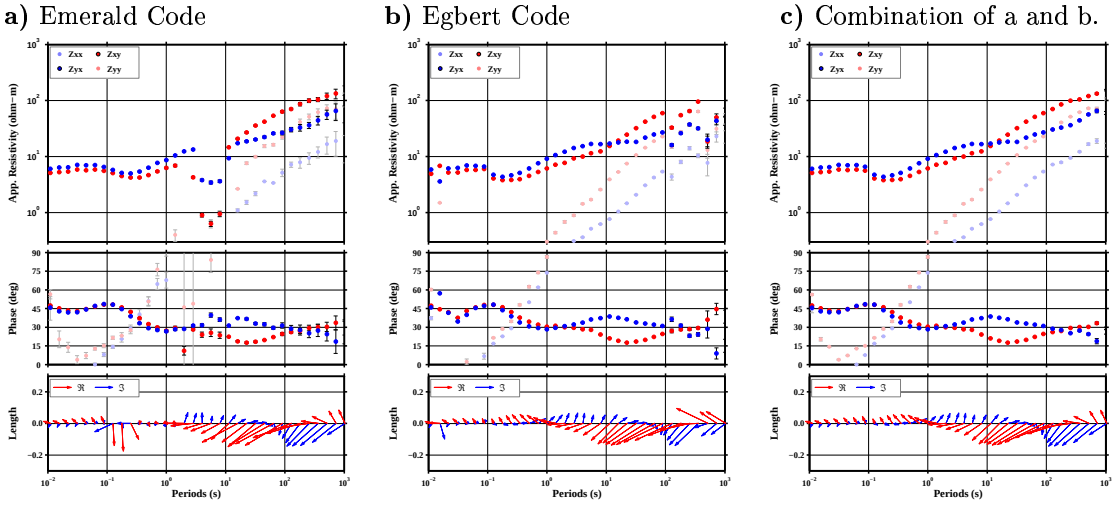

Figure 3: MT impedance tensor and induction vectors at broad-band site 132, located 8 km west of the SAF. **a)** The Emerald code yields stable estimates at periods longer than 100 s, but produces biased transfer functions in the dead band without a manual pre-selection scheme as described in Weckmann et al. (2005). **b)** The Egbert code yields good estimates in the dead band using a remote reference but erratic estimates at long periods (>100s). **c)** The combination of the two methods yields good data for a broad period range.

Data processing and analysis

For processing of time series, we used a combination of the robust remote-reference processing of Egbert and Booker (1986) the robust code of Ritter et al. (1998) (Emerald). Egbert's code yielded superior results in the dead band (0.2-10s), when a good reference site was available. This was the case for almost all broad-band sites due to the great number of simultaneously operated instruments (up to 10 broad-band stations). However, even with a remote reference included, estimated transfer functions were erratic at periods longer than 100s in case of 3 days long broad-band recordings (at long-period sites with recording time longer than 10 days, reliable transfer functions could be estimated also at periods longer than 100s). Hence, there is coherent noise in the data, possibly arising from the BART DC-railway system or from pulsed pipelines. Using the Emerald code and employing the automatic phase criterion (i.e. segments with phases out of the quadrant are rejected in robust stacking; cf. Weckmann et al., 2005) and a coherency threshold of 0.95, stable transfer functions were obtained also for periods longer than 100 s. Hence, it is by a pre-selection criterion possible to determine noisy segments and remove them from subsequent processing. However, to improve the data quality within the dead band, a manual selection in frequency domain (Weckmann et al., 2005) would have been necessary. An example of the transfer functions concatenated from Egbert's code and the Emerald code is shown in Figure 3.

Impedance data as well as induction vectors show a predominant strike direction aligned with the San Andreas Fault zone. We observe, however, 3D effects, mainly at intermediate periods between 10-100s. For an impedance tensor analysis and decomposition, we use the ellipticity criterion of Becken and Burkhardt (2004), which reduces to the classical galvanic distortion analysis in presence of a regional 2D structure. The existence of a 2D structure is inferred from the linear polarisation of principal electric and magnetic fields, which is expressed in terms of linearly polarised columns of the tensor. The coordinate system in which the sum of squared ellipticities weighted with their variances is minimal for a range of periods is determined using an automatic algorithm. This coordinate system is considered as the strike direction if the ellipticities are indeed close to zero and the distortion angles are constant over the given range of periods.

An example of the ellipse parameterisation is shown in Figure 4b for the impedance data of site 020 shown in Figure 4a. Impedances and induction vectors in Figure 4a are rotated to 45° clockwise, i.e. the y-axis is aligned with the SAF. Ellipticities at short periods (<3s) and at long periods (>100s) vanish in this coordinate system. The electric field rotation angles, i.e. the distortion angles, depicted in the lower panel of Figure 4b, are constant over the respective period ranges where the ellipticities vanish, but different at short and at long periods. Therefore, two galvanic distortion matrices should be incorporated to decompose the data: one distortion matrix at short periods and one at long periods. On the other hand, undistorted data do in this case not significantly differ from simply rotated impedance data, which permits an inversion of the rotated impedances directly. At intermediate periods, 3D effects are identified from non-vanishing ellipticities and period dependent distortion angles, which coincides with a slight rotation of induction vectors.

Note, that the estimated strike direction is in good agreement with the induction vectors (though the induction vectors at long periods are strongly influenced by the pacific ocean and therefore do not necessarily reflect the same conductivity anomaly as the impedance data).

Site 020, which has been discussed above, is representative for most of the sites in terms of the dimensionality of the impedance tensor and its rotational properties, although strike directions at short periods are not as consistent along the profile as at long periods. In summary, the distortion analysis and the induction vectors suggests that the rotation angle of $45° \pm 5°$ is appropriate for a 2D interpretation of the short and long period data. The intermediate period range exhibiting 3D effects should be excluded from inversion or given less weight by increasing the error bars.

2D Interpretation

Inversion strategy: We use the 2D smooth inversion code of Mackie et al. (1997) as it is implemented in the Winglink software package. Using this program, we jointly invert the presumed E- and H-polarisation apparent resistivities and phases and the projection of induction vectors onto the profile line. Large error floors,

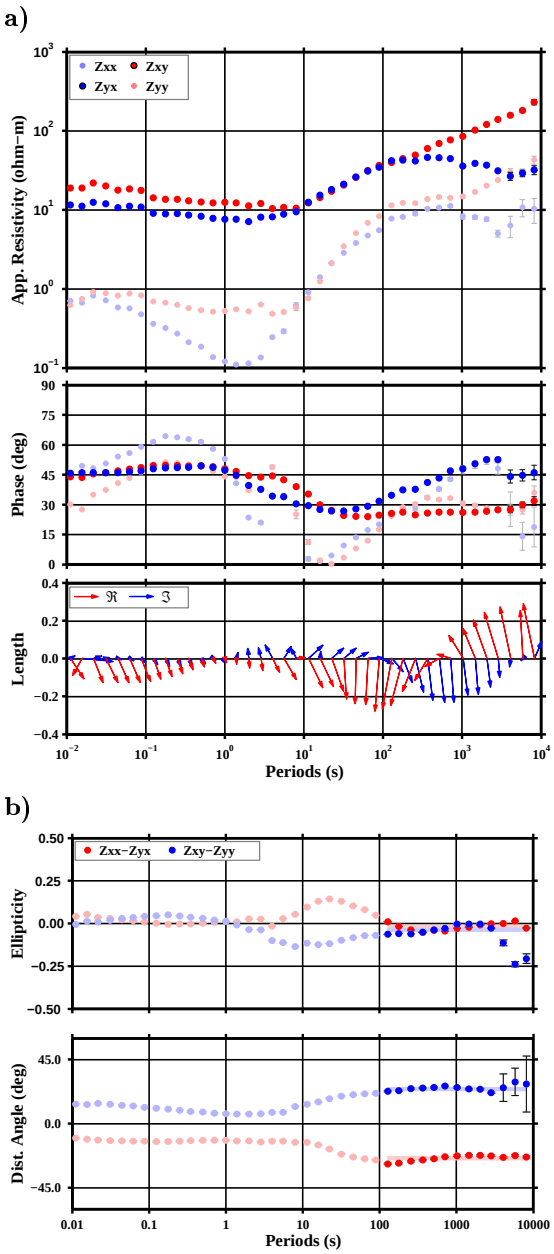

Figure 4: B/LMT site 020, located app. 1 km east of the surface trace of the SAF. **a)** MT apparent resistivities, phases and induction vectors (upper, middle and lower panel, respectively). The coordinate system is rotated to $+45°$, i.e. the $x-$axis is in profile direction the $y-$axis is aligned with the SAF. **b)** Ellipticities and galvanic distortion angles obtained from decomposition of the MT impedance tensor.

assigned to the apparent resistivities (E-Pol.: 100%; H-Pol.: 25%), avoid bias of the model associated with static shift effects. Emphasis was instead put on the phases (2° error floor) and induction vectors (0.02 error floor). The regularisation parameter, trading off between model roughness and data fit, is determined by trial and error.

The choice of the starting model is important in this context, because the ocean effect has to be taken into account. Modelling results as well as the similarity of induction vectors along the profile at periods longer than 2000s suggest, that the effect of the ocean becomes significant at these periods. To reproduce the long-period induction vectors with the pacific ocean as conductive anomaly, the crust between the coast and the measurement area has to be resistive ($> 1000\,\Omega m$). Otherwise, the spatial decay of the anomalous fields induced in the ocean would be too strong and the effect at Parkfield would be underestimated. Therefore, if we did not incorporate a resistive crust in the starting model, the inversion would attempt to simulate the ocean effect with an extremely large, unrealistically conducting anomaly close to the measurement area.

2D Models: Data analysis and 2D modelling results of the new profile data together with existing data from the previous experiments reveal the conductivity structure of the crust from the top to the bottom (cf. Figure 5). We also recover the previous local MT model of Unsworth and Bedrosian (2004), which can now be looked at in a regional context. However, due to the 3D complications described above, there exist currently concurrent versions of the model, which agree in its major features but differ in minor aspects. Therefore, the model in Figure 5 is a preliminary result.

The regional conductivity model clearly shows that the seismically active zone (red dots in Figure 5 indicate the earthquake locations, taken from the latest earthquake catalogue of Thurber & Zhang, personal communication) along the SAF zone is bent around the north-eastern edge of an isolated, large granitic body (Salinian Granite). An upper wedge of the Granite was drilled by the SAFOD main hole; its lateral extensions were previously modelled from surface magnetic anomaly maps. The conductivity model traces the granite down to a

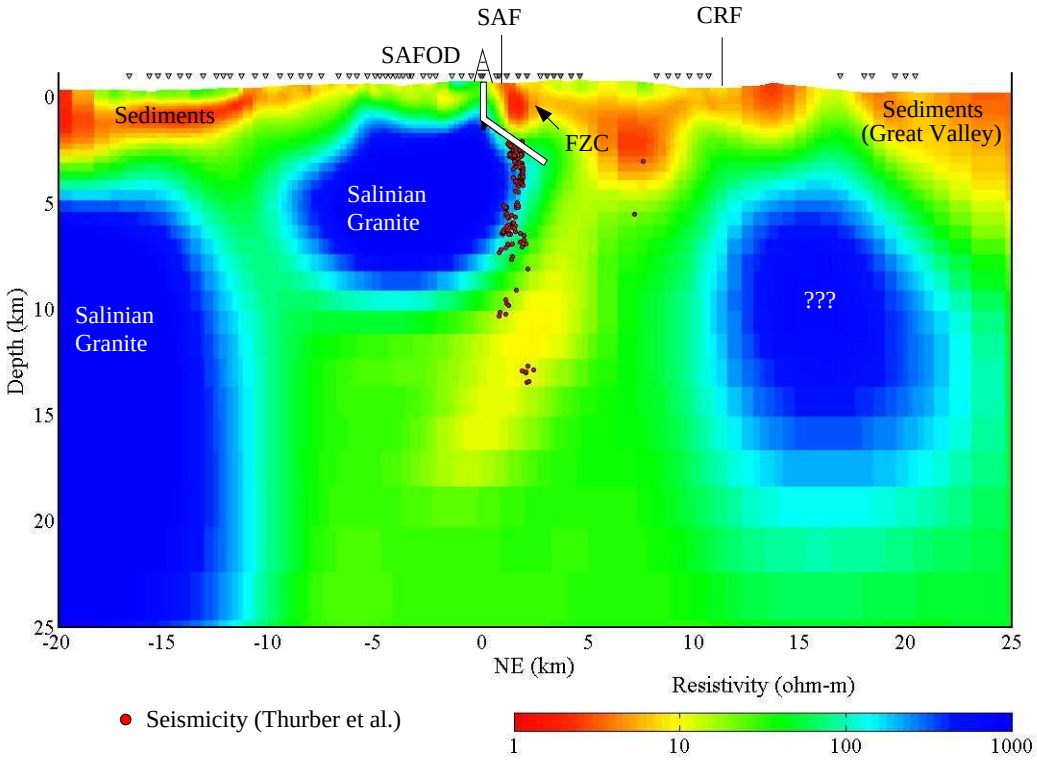

Figure 5: Preliminary resistivity model obtained from joint 2D inversion of E- and H-polarisation apparent resistivities and induction vectors. The SAFOD main hole is indicated with a white patch. Seismicity within 3 km away from the section is depicted with red dots. SAFOD San Andreas Fault Observatory At Depth; SAF San Andreas Fault; CRF Coast Range fault. See text for details.

depth of 8 kilometres and thereby suggests a lithological contrast in the vicinity of or directly at the plane of seismicity.

Modelled conductivities in the brittle portion of the SAF are not high enough for a significantly increased fluid volume and, associated with that, enhanced porosity of fractured rocks directly within the fault zone. This means that either there is no significant increase in the bulk porosity or there is only a narrow zone of increased porosity - too narrow to be resolved with magnetotelluric measurements.

However, we do resolve a series of likely connected conductors within the upper 5km of the crust - one of them being the previously described Fault Zone Conductor of Unsworth and Bedrosian (2004). A broad zone of enhanced conductivity is located two to five kilometres east of the active SAF and extends to a depth of at least $5\,km$. This zone provides a linkage between the surface conductors, in particular the FZC topping the seismic region, and the lower crust. It also provides an apparent link of the Coast Range Fault (15 km to the east) and the SAF at depth.

The middle and lower crust (>10 km) below the SAF zone is generally conductive (<20 ohm-m) in a 20 km wide zone, which is enclosed by the resistive Salinian Granite in the southwest and an isolated resistor to the northeast.

Outlook

In this paper, we focused on technical aspects of the new MT data across the SAF and the generation of a 2D model. Future work comprises (i) a full 3D inversion of the MT array data, (ii) the integration of the MT image with other geophysical models (seismic reflection and refraction), (iii) to understand the meaning of the geophysical models in terms of the mechanics and dynamics of the SAF at depth.

References

Becken, M., Burkhardt, H., 2004. An ellipticity criterion in magnetotelluric tensor analysis. Geophys. J. Int. 159, 69–82.

Egbert, G. D., Booker, J. R., 1986. Robust estimation of geomagnetic transfer functions. Geophys. J. R. astr. Soc. 87, 173–194.

Hickman, S., Zoback, M., Ellsworth, W., 2004. Introduction to special section: Preparing for the San Andreas Fault Observatory at Depth. Geophys. Res. Lett. 31, L12S01.

Hole, J. A., Ryberg, T., Sharma, A. K., Fuis, S. G., 2004. Seismic velocity structure from a refraction - reflection survey across the san andreas fault at safod. AGU Fall meeting, San Francisco.

Mackie, R., Rieven, S., Rodi, W., Jul. 1997. Users manual and software documentation for two-dimensional inversion of magnetotelluric data. GSY-USA, Inc., 2261 Market St., Suite 643, San Francisco, CA 94114, User Documentation.

Ritter, O., Junge, A., Dawes, G. J. K., 1998. New equipment and processing for magnetotelluric remote reference observations. Geophys. J. Int. 132, 535–548.

Ryberg, T., Hole, J. A., Fuis, G. S., 2004. Controlled source p and s wave tomography at safod. AGU Fall meeting, San Francisco.

Unsworth, M. J., Bedrosian, P., 2004. Electrical Resistivity structure at the SAFOD site from magnetotelluiric exploration. Geophys. Res. Lett. 31, L12S05.

Unsworth, M. J., Malin, P. E., Egbert, G. D., Booker, J. R., 1997. Internal structure of the San Andreas fault at Parkfield, California. Geology 25, 359–362.

Weckmann, U., Magunia, A., Ritter, O., 2005. Effective noise separation for magnetotelluric single site data processing using a frequency domain selection scheme. Geophys. J. Int. 162 (3), 635–652.